7-15-2009

# X-Ray Photoemission Analysis of Chemically Treated GaTe Semiconductor Surfaces for Radiation Detector Applications

A. J. Nelson

A. M. Conway

B. W. Sturm

E. M. Behymer

C. E. Reinhardt

***See next page for additional authors***



## Publication Info

Published in *Journal of Applied Physics*, Volume 106, Issue 2, 2009, pages 023717-1-023717-5.

Nelson, A. J., Conway, A. M., Sturm, B. W., Behymer, E. M., Reinhardt, C. E., Nikolic, R. J., Payne, S. A., Pabst, G., & Mandal, K. C. (15 July 2009). X-ray photoemission analysis of chemically treated GaTe semiconductor surfaces for radiation detector applications. *Journal of Applied Physics*, 106(2), #023717.
http://dx.doi.org/10.1063/1.3176478
http://scitation.aip.org/content/aip/journal/jap/106/2/10.1063/1.3176478

**Author(s)**
A. J. Nelson, A. M. Conway, B. W. Sturm, E. M. Behymer, C. E. Reinhardt, R. J. Nikolic, S. A. Payne, G. Pabst, and K. C. Mandal

# X-ray photoemission analysis of chemically treated GaTe semiconductor surfaces for radiation detector applications

A. J. Nelson, A. M. Conway, B. W. Sturm, E. M. Behymer, C. E. Reinhardt, R. J. Nikolic, S. A. Payne, G. Pabst, and K. C. Mandal

Citation: Journal of Applied Physics **106**, 023717 (2009); doi: 10.1063/1.3176478
View online: http://dx.doi.org/10.1063/1.3176478
View Table of Contents: http://scitation.aip.org/content/aip/journal/jap/106/2?ver=pdfcov
Published by the AIP Publishing



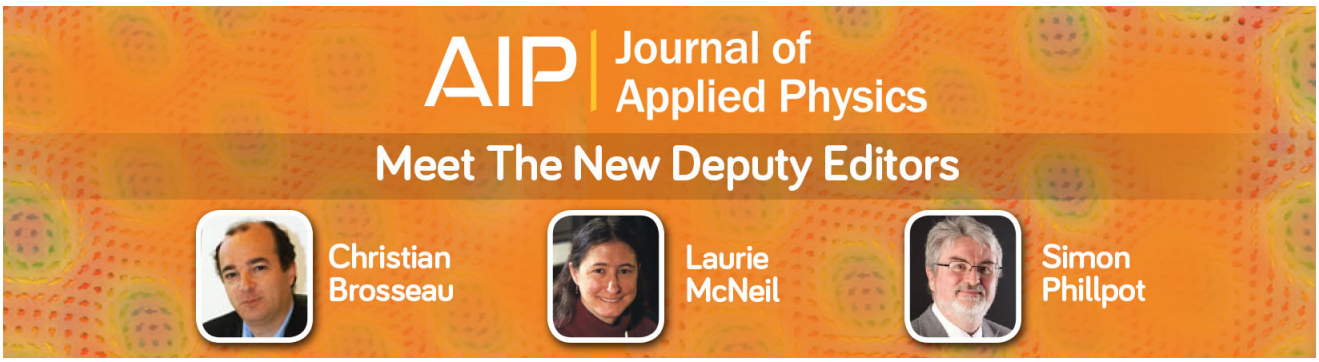

# X-ray photoemission analysis of chemically treated GaTe semiconductor surfaces for radiation detector applications

A. J. Nelson,[1,a)] A. M. Conway,[1] B. W. Sturm,[1] E. M. Behymer,[1] C. E. Reinhardt,[1] R. J. Nikolic,[1] S. A. Payne,[1] G. Pabst,[2] and K. C. Mandal[2]
[1]*Lawrence Livermore National Laboratory, Livermore, California 94550, USA*
[2]*EIC Laboratories, Inc., 111 Downey Street, Norwood, Massachusetts 02062, USA*

(Received 29 May 2009; accepted 9 June 2009; published online 27 July 2009)

The surface of the layered III-VI chalcogenide semiconductor GaTe was subjected to various chemical treatments commonly used in device fabrication to determine the effect of the resulting microscopic surface composition on transport properties. Various mixtures of $H_3PO_4$:$H_2O_2$:$H_2O$ were accessed and the treated surfaces were allowed to oxidize in air at ambient temperature. High-resolution core-level photoemission measurements were used to evaluate the subsequent chemistry of the chemically treated surfaces. Metal electrodes were created on laminar (cleaved) and nonlaminar (cut and polished) GaTe surfaces followed by chemical surface treatment and the current versus voltage characteristics were measured. The measurements were correlated to understand the effect of surface chemistry on the electronic structure at these surfaces with the goal of minimizing the surface leakage currents for radiation detector devices. © *2009 American Institute of Physics*.
[DOI: 10.1063/1.3176478]

## I. INTRODUCTION

The layered III-VI chalcogenide semiconductor GaTe has potential for room temperature gamma ray spectroscopy applications due to its 1.68 eV band gap at 300 K and high atomic numbers.[1,2] Attempts to fabricate working room temperature radiation detectors using high-resistivity GaTe substrates have precipitated the need to engineer the chemical states at the metal/semiconductor interface. Controlling the oxidation state at this interface will impact the device transport properties and thus an appropriate surface preparation needs to be developed.

Mechanical polishing followed by chemical etching is routinely employed for surface preparation prior to device fabrication. However, alternative surface preparation methods need to address surface passivation of defect states. Surface passivation of III-V compound semiconductor surfaces is well documented[3] as a means to address the detrimental effects coming from high-density surface states and related Fermi level pinning. Similar surface treatments related to II-VI binary and I-III-VI ternary semiconductor devices have been explored only recently.[4–10]

In this work, various wet chemical treatments with $H_3PO_4$:$H_2O_2$:$H_2O$, $H_3PO_4$:$H_2O$, and $H_2O_2$:$H_2O$ were accessed. The chemical processing of the GaTe surface is examined in detail by interrupting the treatment cycle and characterizing with monochromatic x-ray photoelectron spectroscopy (XPS) to examine the surface reactions associated with each separate chemical treatment. The treated surfaces were allowed to oxidize in air at ambient temperature for timed intervals and characterizing the surface after each timed exposure in order to monitor the growth of any oxide layer. Current-voltage (*I-V*) measurements were acquired after metalizing, chemically treating the exposed surface, and correlating the results with the surface chemistry.

## II. EXPERIMENTAL

GaTe crystals were grown at EIC Laboratories using stoichiometric amounts of high-purity (7*N*) Ga and zone refined Te as starting materials to make a homogeneous polycrystalline ingot. The polycrystalline ingot was encapsulated in Struers Epofix for metallographic sample preparation. Sequential polishing of the GaTe with finer and finer diamond paste followed by colloidal silica resulted in a surface with a mirror finish and rms surface roughness of 20 nm as determined with Zygo optical interferometry. Wet etching of the polished GaTe laminar surface was performed using various mixtures of $H_3PO_4$, $H_2O_2$, and $H_2O$. Specifically, $H_3PO_4$:$H_2O_2$:$H_2O$ with the ratio of 1:1:10 by volume, respectively, $H_3PO_4$:$H_2O$ (1:10) and $H_2O_2$:$H_2O$ (1:10). Following each treatment cycle, the samples were rinsed in deionized water and blown dry with $N_2$. XPS was used to investigate the surface chemistry after each treatment cycle in an effort to understand the effect of surface composition on room temperature radiation detector performance.

XPS analysis was performed on a PHI Quantum 2000 system using a focused monochromatic Al $K\alpha$ x-ray (1486.7 eV) source for excitation and a spherical section analyzer. The instrument has a 16-element multichannel detection system. A 100 $\mu$m diameter x-ray beam was used for analysis. The x-ray beam is incident normal to the sample and the x-ray detector is at 45° away from the normal. The pass energy was 23.5 eV giving an energy resolution of 0.3 eV that when combined with the 0.85 eV full width at half maximum (FWHM) Al $K\alpha$ linewidth gives a resolvable XPS peak width of 1.2 eV FWHM. Deconvolution of nonresolved peaks was accomplished using Multipak 6.1A (PHI) curve fitting routines. The collected data were referenced to an en-

[a)]Electronic mail: nelson63@llnl.gov.

 

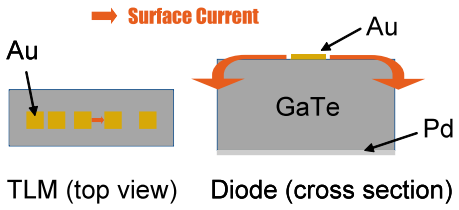


FIG. 1. (Color online) Schematic diagram of TLM patterns and diodes used in surface treatment experiments.

ergy scale with binding energies for Cu $2p_{3/2}$ at $932.72 \pm 0.05$ eV and Au $4f_{7/2}$ at $84.01 \pm 0.05$ eV. Binding energies were also referenced to the C 1*s* photoelectron line arising from adventitious carbon at 284.8 eV. Low energy electrons and argon ions were used for specimen neutralization.

The effect of the aforementioned chemical treatments on surface conductivity was studied on both the nonlaminar and laminar surface of GaTe sample. The nonlaminar surface was prepared using the cutting and polishing procedure described above and the laminar surface was prepared by cleaving. Gold electrode patterns were fabricated using standard photolithography and lift off processes. Transmission line method (TLM) patterns were used to evaluate the change in sheet resistance of the material, and circular diode patterns were used to measure the change in bulk current after each treatment which is shown schematically in Fig. 1. Current versus voltage measurements were performed on the TLM patterns and diodes as fabricated, after 1 min in $H_3PO_4:H_2O$ (1:10), after 1 min in $H_2O_2$ (30% dilute), and finally a $H_3PO_4:H_2O_2:H_2O$ (1:1:10) treatment for 5 min.

A wet etching experiment of GaTe was performed using a mixture of $H_3PO_4$, $H_2O_2$, and $H_2O$ with the ratio of 1:1:10 by volume, respectively. To create a pattern on the sample to use as an etch mask, photolithography followed by e-beam evaporation of 200 nm of Au and finally lift off of the unwanted metal portions were performed on a laminar face of the GaTe sample. The experiment consisted of exposing the sample to the etchant for durations of 1, 2, and 5 min and measuring the step height with a surface profilometer in between each etch step to determine the etch rate and surface roughness. This etchant functions by oxidizing the GaTe via the $H_2O_2$ followed by etching with $H_3PO_4$. The etch rate of the GaTe nonlaminar surface for various concentrations of the solution (abscissa), the effect of stirring, and crystallographic direction was determined. In all experiments, the reaction was conducted in room light and the solution was at room temperature.

TABLE I. Relative XPS surface compositional analysis (at %) of the $H_3PO_4:H_2O_2:H_2O$ treated and air-exposed GaTe.

| Sample | Ga | Te | O | Ga/Te ratio |
|---|---|---|---|---|
| As-received | 9.8 | 28.6 | 61.6 | 0.34 |
| 1 min $H_3PO_4:H_2O_2:H_2O$ | 5.3 | 10.5 | 84.2 | 0.50 |
| 3 min $H_3PO_4:H_2O_2:H_2O$ | 11.3 | 32.5 | 56.2 | 0.35 |
| 5 min $H_3PO_4:H_2O_2:H_2O$ | 18.1 | 58.7 | 23.2 | 0.31 |
| 5 min air exposure | 18.2 | 45.1 | 36.7 | 0.40 |
| 10 min air exposure | 8.5 | 31.1 | 60.4 | 0.27 |
| 20 min air exposure | 4.5 | 41.4 | 54.1 | 0.11 |
| 40 min air exposure | 4.0 | 38.8 | 57.2 | 0.10 |
| 80 min air exposure | 7.9 | 37.2 | 54.9 | 0.21 |

TABLE II. Relative XPS surface compositional analysis (at %) of the $H_3PO_4:H_2O$ treated GaTe.

| Sample | Ga | Te | O | Ga/Te ratio |
|---|---|---|---|---|
| As-received | 9.8 | 28.6 | 61.6 | 0.34 |
| 1 min $H_3PO_4:H_2O$ | 6.8 | 34.1 | 59.1 | 0.20 |
| 5 min in air | 6.2 | 35.5 | 58.3 | 0.17 |
| 15 min in air | 11.5 | 29.9 | 58.6 | 0.38 |
| 35 min in air | 7.4 | 38.6 | 54.0 | 0.19 |
| 75 min in air | 5.7 | 37.7 | 56.6 | 0.15 |

## III. RESULTS AND DISCUSSION

XPS survey spectra of the as-treated GaTe laminar surfaces were acquired to determine surface stoichiometry and impurity concentrations. The quantitative surface compositional analyses and elemental ratios are summarized in Tables I–III. The Ga/Te ratio indicates that the as-received laminar surface is Te rich. Compositional analysis following the 5 min $H_3PO_4:H_2O_2:H_2O$ treatment reveals less oxygen and a Ga/Te ratio indicative of a Te-rich surface. The 1 min $H_3PO_4:H_2O$ treatment also results in a Te-rich surface while the $H_2O_2:H_2O$ treatment initially results in a more stoichiometric oxidized surface. These as-treated surfaces were exposed to air and allowed to react then further characterized as described below.

Photoemission measurements on the Ga 2*p*, Te 3*d*, and O 1*s* core lines were used to further evaluate the chemical bonding on the as-treated surfaces at each cycle of the process and after subsequent oxidation. Beginning with the as-received polished surface, the Ga $2p_{3/2}$ peak binding energy is 1118.4 eV, which is representative of $Ga_2O_3$. The Te 3*d* spectrum shown in Fig. 2 for the as-received GaTe surface shows two sets of Te $3d_{5/2,3/2}$ spin-orbit pairs. The higher binding energy Te $3d_{5/2}$ peak at 576.3 eV represents $Te^{4+}$ in $TeO_2$ ($E_g = 3.5$ eV) and the lower binding energy peak at 573 eV represents lattice bound Te in GaTe.[10,11] In addition, the O 1*s* peak has two components with 530.8 and 532.8 eV binding energies attributed to $Ga_2O_3$ and $TeO_2$, respectively. The binding energies for the photoelectron peaks are summarized in Table IV.

After 1 min in the $H_3PO_4:H_2O_2:H_2O$ solution, the GaTe surface becomes fully oxidized as evidenced by the Te $3d_{5/2}$ peak at 576.4 eV indicative of $Te^{4+}$ in $TeO_2$ and the absence of the lower binding energy component. The lower binding energy Te $3d_{5/2}$ peak reappears following 3 min in the

TABLE III. Relative XPS surface compositional analysis (at %) of the $H_2O_2:H_2O$ treated GaTe

| Sample | Ga | Te | O | Ga/Te ratio |
|---|---|---|---|---|
| As-received | 9.8 | 28.6 | 61.6 | 0.34 |
| 1 min $H_2O_2:H_2O$ | 17.9 | 20.4 | 61.7 | 0.88 |
| 3 min $H_2O_2:H_2O$ | 29.8 | 13.9 | 56.3 | 2.14 |
| 5 min $H_2O_2:H_2O$ | 28.8 | 14.2 | 57.0 | 2.03 |

TABLE IV. Summary of XPS binding energies (eV) for the $H_3PO_4:H_2O_2:H_2O$ processed and air-exposed GaTe.

| GaTe | Ga $2p_{3/2}$ | Te $3d_{5/2}$ | O $1s$ |
|---|---|---|---|
| As received | 1118.4 | 573.0, 576.3 | 530.8, 532.8 |
| 1 min etch | 1118.4 | 576.4 | 531.8, 533.1 |
| 3 min etch | 1118.9 | 573.0, 576.6 | 531.4, 533.0 |
| 5 min etch | 1119.4 | 572.9 | ··· |
| 5 min air exposure | 1119.2 | 573.1 | ··· |
| 10 min air exposure | 1119.4 | 573.2, 576.9 | ··· |
| 20 min air exposure | 1119.3 | 573.1, 576.8 | 531.0, 532.3 |
| 40 min air exposure | 1119.4 | 573.1, 576.5 | 531.0, 532.3 |
| 80 min air exposure | 1119.1 | 573.0, 576.4 | 530.6, 532.1 |

$H_3PO_4:H_2O_2:H_2O$ solution. Finally, after 5 min in the $H_3PO_4:H_2O_2:H_2O$ solution, the GaTe surface is oxide free as evidenced by the sole Te $3d_{5/2}$ peak at 572.9 eV. Based on this data we conclude that the $H_3PO_4:H_2O_2:H_2O$ solution first oxidizes the GaTe surface and then completely removes the oxide, leaving a pristine surface ideal for metal contact application.

The stability of the $H_3PO_4:H_2O_2:H_2O$ treated GaTe surface was quantitatively measured by allowing the etched GaTe surface to oxidize in air at ambient temperature for timed intervals and characterizing the surface after each timed exposure. Monitoring the growth of the oxide was thus accomplished using the components of the Te $3d_{5/2}$ peak and their respective binding energies.

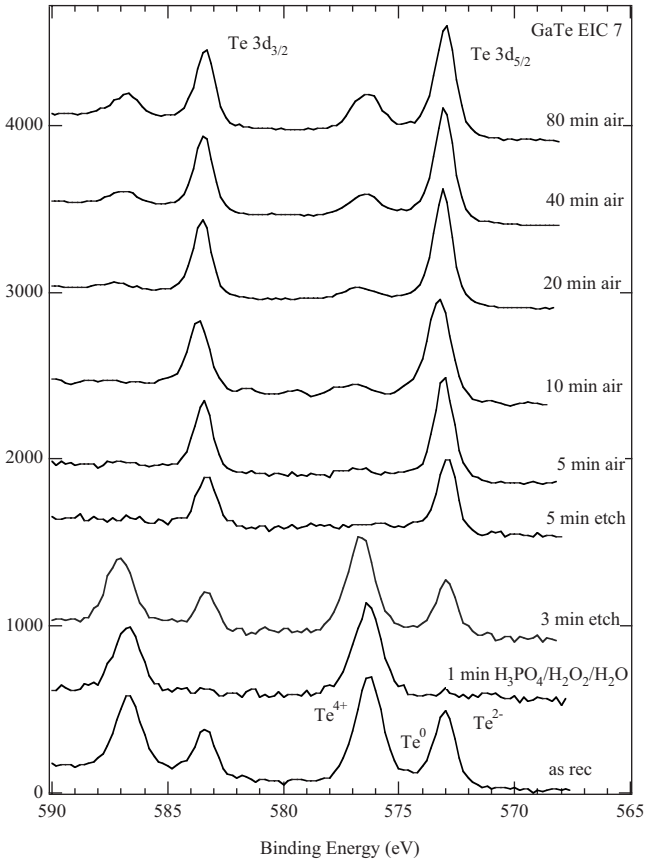


FIG. 2. XPS Te $3d$ spectra for $H_3PO_4:H_2O_2:H_2O$ etched and oxidized GaTe.

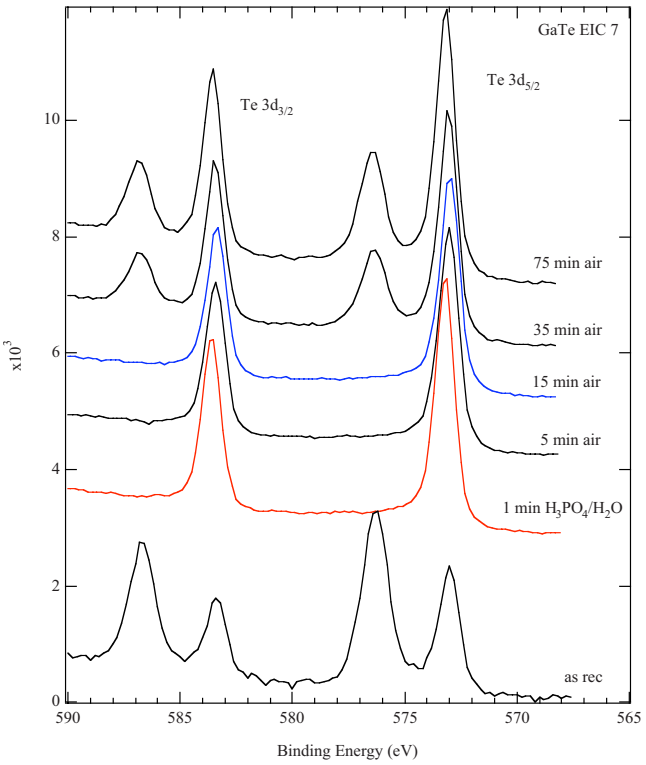


FIG. 3. (Color online) XPS Te $3d$ spectra for $H_3PO_4:H_2O$ etched and oxidized GaTe.

From Fig. 2 we note that minimal oxide growth has occurred on the etched GaTe surface after 5 min in ambient air. However, after 10 min in air, a small Te $3d_{5/2}$ component indicative of $TeO_2$ begins to appear at 576.9 eV. This oxide

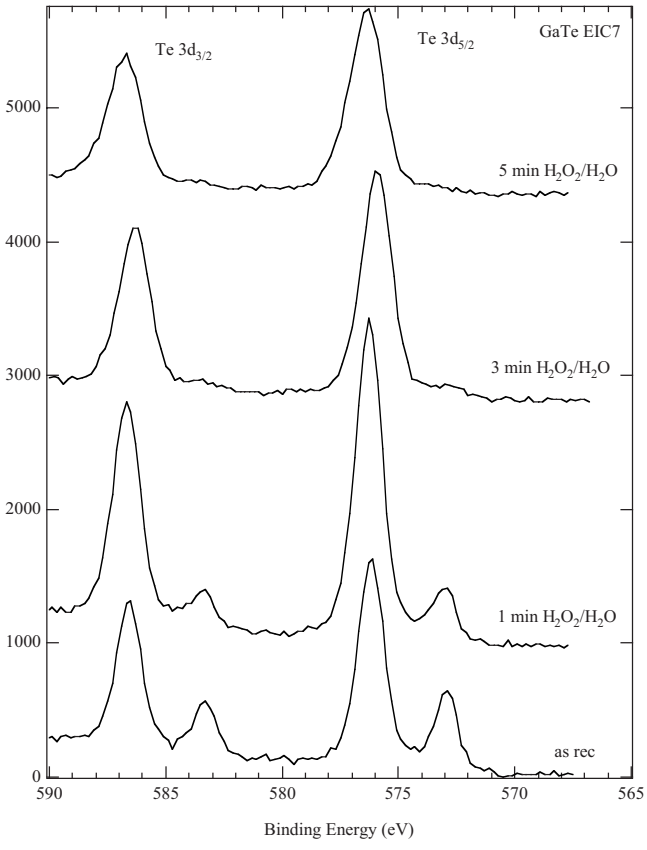


FIG. 4. XPS Te $3d$ spectra for $H_2O_2:H_2O$ oxidized GaTe.

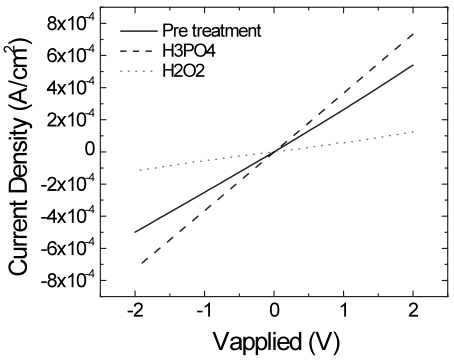


FIG. 5. Current vs voltage characteristics of 100 $\mu$m diameter Au–GaTe–Au diodes before and after various treatments.

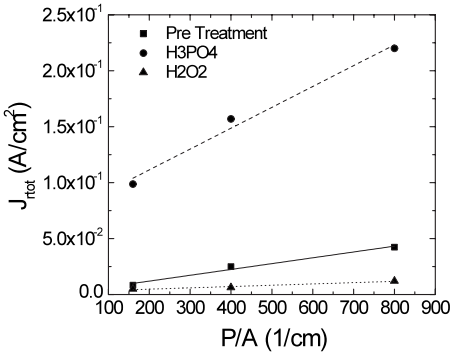


FIG. 7. Current density vs electrode periphery to area ratio for various chemical treatments.

peak continues to grow after each air exposure but never attains its original "as-received" intensity. This data suggests that the $H_3PO_4:H_2O_2:H_2O$ solution treatment initially passivates the GaTe surface.

To further elucidate the oxidation/reduction mechanism of the $H_3PO_4:H_2O_2:H_2O$ solution on the GaTe surface, $H_3PO_4:H_2O$ and $H_2O_2:H_2O$ solutions were used separately. Figure 3 shows the progression of Te surface chemical bonding at each timed treatment cycle. After 1 min in the $H_3PO_4:H_2O$ solution, the GaTe surface is oxide free as evidenced by the sole Te $3d_{5/2}$ peak at 573.2 eV. Allowing the surface to oxidize in air at ambient temperature for timed intervals, we note that minimal oxide growth has occurred on the etched GaTe surface after 15 min in ambient air. However, after 35 min in air, a Te $3d_{5/2}$ component indicative of $TeO_2$ begins to appear at 576.3 eV. This oxide peak continues to grow after further air exposure but again never attains its original as-received intensity. This data suggests that the $H_3PO_4:H_2O$ solution alone can be used to effectively passivate the GaTe surface.

The progression of Te surface chemical bonding for the $H_2O_2:H_2O$ solution is presented in Fig. 4. After 1 min in the $H_2O_2:H_2O$ solution, the as-received GaTe surface is further oxidized as evidenced by the increased intensities of the Te $3d_{5/2}$ peak indicative of surface oxide. Compositional analysis revealed that this is a more stoichiometric surface than the as-received surface. A 3 or 5 min treatment in $H_2O_2:H_2O$ yields a fully oxidized surface initially forming a mixture of $Ga_2O_3/TeO_2$ or $GaTeO_3$ that may prove ideal for Schottky contacts on GaTe.

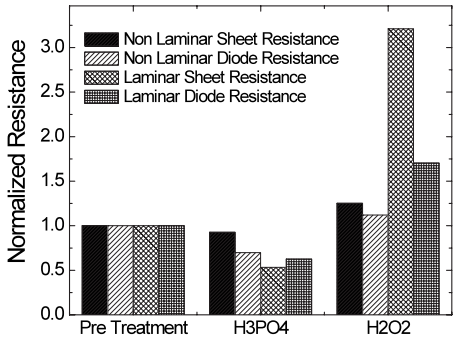


FIG. 6. Normalized sheet and diode resistances after the various surface treatments for laminar and nonlaminar surfaces. The resistances are normalized to the pre-surface treatment resistance for each case.

The measurements of the *I-V* characteristics for these $H_3PO_4:H_2O_2:H_2O$, $H_3PO_4:H_2O$, and $H_2O_2:H_2O$ treated surfaces reveals that Au forms an Ohmic contact (Fig. 5). A comparison of the sheet resistance and diode resistance after each chemical treatment for the laminar and nonlaminar surface is shown in Fig. 6. Similar trends are observed for both measurements, namely, after phosphoric acid treatment the effective resistance decreases, possibly due to the removal of a passivating native oxide as was shown above using XPS. Following the hydrogen peroxide treatment, a stable surface $TeO_x$ is formed which increases the effective resistance by acting as surface passivation. The surface and bulk components of the diode current for the laminar diodes were determined by measuring electrodes of various diameters, using the relationship

$$J_{\text{rtot}} = J_a + J_p * P/A, \tag{1}$$

where $J_{\text{rtot}}$ is the total current density in $A/cm^2$, $J_a$ is bulk component of the current density in $A/cm^2$, $J_p$ is the periphery component in A/cm, $P$ is the electrode periphery in centimeter, and $A$ is the electrode area in $cm^2$. The components are determined by plotting the total electrode current density at a fixed voltage as a function of $P$ to $A$ ratio for various size electrodes (Fig. 7), where the slope is equal to the periphery component and the intercept is the bulk component, show in Table V. The bulk component stays relatively constant (maximum two times change) with surface treatment whereas the periphery component varies by ten times.

The etch rates for various concentrations of etchant are shown in Fig. 8. We find that the etch rate was 0–50 Å/s depending on chemical concentration, and that the etch rate was not influenced by the crystallographic orientation in the nonlaminar direction. In addition, we did not observe a statistically relevant increase in etch rate with stirring, suggesting the kinetics are not diffusion-limited but rather reaction limited. The etch rate along the laminar direction is three

TABLE V. Area and periphery components of current density for treated samples.

| Surface treatment | $J_a$ | $J_p$ |
|---|---|---|
| Pretreatment | 0.001 59 | $5.205\ 08 \times 10^{-5}$ |
| $H_3PO_4$ | 0.074 14 | $1.8631 \times 10^{-4}$ |
| $H_2O_2$ | 0.002 48 | $1.1642 \times 10^{-5}$ |

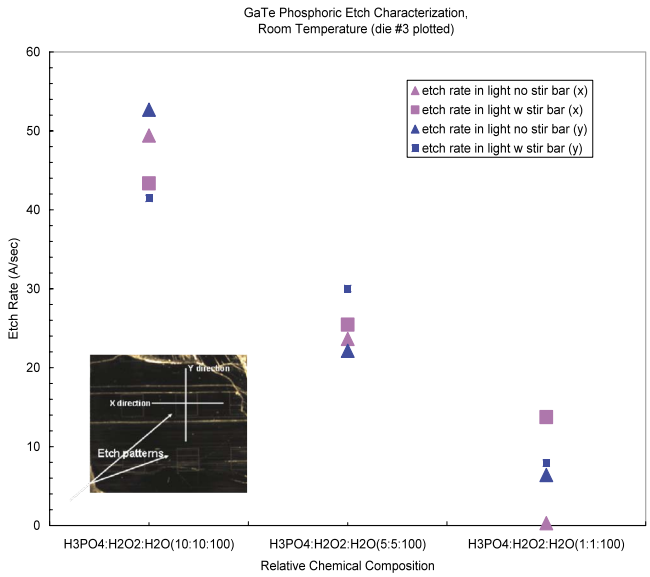


FIG. 8. (Color online) Etch rate for the nonlaminar surface and the effect of chemical concentration, crystallographic direction, and use of stirring. Inset: low magnification SEM image of the GaTe surface used for wet chemical etching experiments. A square photoresist pattern was used for surface profilometry to determine the etch rate.

times faster than the nonlaminar direction as evidenced by the scanning electron microscopy (SEM) of the post etch electrode in Fig. 9.

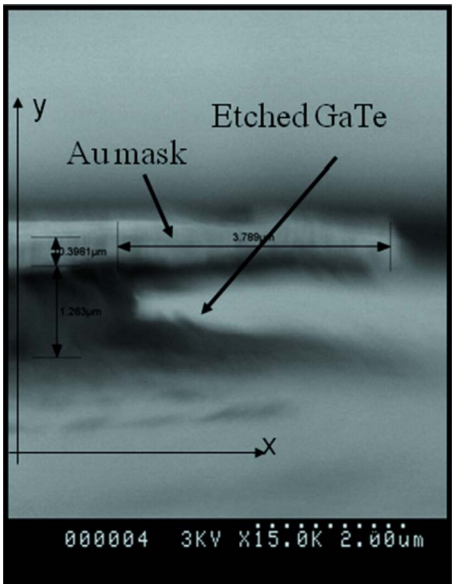


FIG. 9. (Color online) SEM picture of $H_3PO_4:H_2O_2:H_2O$ (1:1:10) etched GaTe.

## IV. CONCLUSIONS

Wet chemical treatments can be used to affect GaTe surface chemistry and oxide formation. Various mixtures of $H_3PO_4:H_2O_2:H_2O$ were accessed and the treated surfaces were allowed to oxidize in air at ambient temperature. High-resolution photoemission measurements on the Ga 2*p*, Te 3*d*, and O 1*s* core lines were used to evaluate the subsequent chemistry of the chemically treated surfaces. The measured *I-V* characteristics were correlated with XPS results to understand the effect of surface chemistry on the electronic structure at these surfaces with the goal of minimizing the surface leakage currents for radiation detector devices. Fabrication of room temperature semiconductor radiation detectors should include thoughts on optimizing the metal contact to oxide/semiconductor structure for Schottky barrier engineering, as well as to reduce surface leakage currents.

## ACKNOWLEDGMENTS

The authors would like to thank J. Go and E. Sedillo for metallographic sample preparation. This work was performed under the auspices of the U.S. Department of Energy by Lawrence Livermore National Laboratory under Contract No. DE-AC52-07NA27344 and by the Department of Homeland Security, Domestic Nuclear Detection Office under Contract HSHQDC-07-C-00034.

[1]M. Abdel Rahman and A. E. Belal, J. Phys. Chem. Solids **61**, 925 (2000).
[2]A. M. Conway, C. E. Reinhardt, R. J. Nikolic, A. J. Nelson, T. F. Wang, K. J. Wu, S. A. Payne, A. Mertiri, G. Pabst, R. Roy, K. C. Mandal, P. Bhattacharya, Y.-L. Cui, M. Groza, and A. Burger, in IEEE Nuclear Science Symposium Conference Record, 2007. NSS '07, Vol. 2, pp. 1551–1555.
[3]H. Hasegawa and M. Akazawa, Appl. Surf. Sci. **255**, 628 (2008).
[4]A. J. Nelson, C. R. Schwerdtfeger, G. C. Herdt, D. King, M. Contreras, and K. Ramanathan, J. Vac. Sci. Technol. A **15**, 2058 (1997).
[5]A. J. Nelson, L. Gregoratti, E. Chagarov, D. Lonza, M. Marsi, and M. Kiskinova, Appl. Surf. Sci. **140**, 208 (1999).
[6]K.-T. Chen, D. T. Shi, H. Chen, B. Granderson, M. A. George, W. E. Collins, and A. Burger, J. Vac. Sci. Technol. A **15**, 850 (1997).
[7]S. Wenbin, W. Kunshu, M. Jiahua, T. Jianyong, Z. Qi, and Q. Yongbiao, Semicond. Sci. Technol. **20**, 343 (2005).
[8]V. G. Ivanits'ka, P. Moravec, J. Franc, Z. F. Tomashik, P. I. Feychuk, V. M. Tomashik, L. P. Shcherbak, K. Masek, and P. Hoschl, J. Electron. Mater. **36**, 1021 (2007).
[9]L. Qiang and J. Wanqi, Nucl. Instrum. Methods Phys. Res. A **562**, 468 (2006).
[10]A. J. Nelson, A. M. Conway, C. E. Reinhardt, J. L. Ferreira, R. J. Nikolic, and S. A. Payne, Mater. Lett. **63**, 180 (2009).
[11]O. A. Balitskii and W. Jaegermann, Mater. Chem. Phys. **97**, 98 (2006).